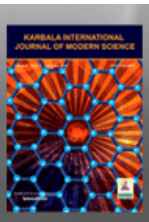

Karbala International Journal of Modern Science

Volume 11 | Issue 2 Article 4

Highly Regenerable Magnetic Sulfonated Chitosan Crosslinked with Glutaraldehyde Composite beads (Iron sand/NaSO3-Chi-G) for Aqueous Mercury Removal

Fathurrahmi Fathurrahmi
Department of Chemistry, Faculty of Mathematics and Natural Sciences, Universitas Syiah Kuala, Kopelma Darussalam, Banda Aceh 23111, Indonesia

Rahmi Rahmi
Department of Chemistry, Faculty of Mathematics and Natural Sciences, Universitas Syiah Kuala, Kopelma Darussalam, Banda Aceh 23111, Indonesia, rahmi@usk.ac.id

Lelifajri Lelifajri
Department of Chemistry, Faculty of Mathematics and Natural Sciences, Universitas Syiah Kuala, Kopelma Darussalam, Banda Aceh 23111, Indonesia

Anggun Sixthia Wulan Ayu
Department of Chemistry, Faculty of Mathematics and Natural Sciences, Universitas Syiah Kuala, Kopelma Darussalam, Banda Aceh 23111, Indonesia

Muhammad Iqhrammullah
Department of Chemistry, Faculty of Mathematics and Natural Sciences, Universitas Syiah Kuala, Kopelma Darussalam, Banda Aceh 23111, Indonesia

Recommended Citation

Fathurrahmi, Fathurrahmi; Rahmi, Rahmi; Lelifajri, Lelifajri; Ayu, Anggun Sixthia Wulan; and Iqhrammullah, Muhammad (2025) "Highly Regenerable Magnetic Sulfonated Chitosan Crosslinked with Glutaraldehyde Composite beads (Iron sand/NaSO3-Chi-G) for Aqueous Mercury Removal," *Karbala International Journal of Modern Science*: Vol. 11 : Iss. 2 , Article 4.
Available at: https://doi.org/10.33640/2405-609X.3401

Highly Regenerable Magnetic Sulfonated Chitosan Crosslinked with Glutaraldehyde Composite beads (Iron sand/NaSO3-Chi-G) for Aqueous Mercury Removal

Abstract

We developed a novel adsorbent from sulfonated, glutaraldehyde-crosslinked chitosan embedded with magnetic iron sand. The adsorbent was synthesized through a two-step process: (1) sulfonation with $N(SO_3Na)_3$ to introduce sulfonate groups, and (2) crosslinking with glutaraldehyde to enhance structural stability. The optimal formulation, containing 43.5% iron sand and crosslinked with 0.17 M glutaraldehyde, exhibited the highest Hg^{2+} adsorption capacity (30.74 mg/g) at pH 3. The adsorbents were characterized using Scanning Electron Microscopy (SEM), Fourier transform infra-red spectroscopic (FT-IR), and X-ray diffraction (XRD) techniques. Adsorption equilibrium was achieved within 60 minutes, and isotherm modeling showed that the process followed the Freundlich model ($R^2 = 0.98$). The adsorbent demonstrated excellent reusability, maintaining its Hg^{2+} adsorption capacity (49.98 ± 0.06 mg/g initially to 49.82 ± 0.02 mg/g after five cycles). Additionally, it effectively removed nearly 100% of mercury from real contaminated water samples. In conclusion, magnetic sulfonated chitosan crosslinked with glutaraldehyde is a highly effective solution for mercury remediation in practical applications.

Keywords

Chitosan; Crosslinking; Hg; Regeneration; Isotherm

RESEARCH PAPER

Highly Regenerable Magnetic Sulfonated Chitosan Crosslinked With Glutaraldehyde Composite Beads (Iron Sand/$NaSO_3$-Chi-G) for Aqueous Mercury Removal

Fathurrahmi [a], Rahmi [a,*], Lelifajri [a], Anggun S. Wulan Ayu [a], Muhammad Iqhrammullah [a,b]

[a] Department of Chemistry, Faculty of Mathematics and Natural Sciences, Universitas Syiah Kuala, Kopelma Darussalam, Banda Aceh 23111, Indonesia
[b] Department of Life Sciences and Chemistry, Jacobs University Bremen, Bremen 28759, Germany

Abstract

We developed a novel adsorbent from sulfonated, glutaraldehyde-crosslinked chitosan embedded with magnetic iron sand. The adsorbent was synthesized through a two-step process: (1) sulfonation with $N(SO_3Na)_3$ to introduce sulfonate groups, and (2) crosslinking with glutaraldehyde to enhance structural stability. The optimal formulation, containing 43.5 % iron sand and crosslinked with 0.17 M glutaraldehyde, exhibited the highest Hg^{2+} adsorption capacity (30.74 mg/g) at pH 3. The adsorbents were characterized using Scanning Electron Microscopy (SEM), Fourier transform infra-red spectroscopic (FT-IR), and X-ray diffraction (XRD) techniques. Adsorption equilibrium was achieved within 60 min, and isotherm modeling showed that the process followed the Freundlich model ($R^2 = 0.98$). The adsorbent demonstrated excellent reusability, maintaining its Hg^{2+} adsorption capacity (49.98 ± 0.06 mg/g initially to 49.82 ± 0.02 mg/g after five cycles). Additionally, it effectively removed nearly 100 % of mercury from real contaminated water samples. In conclusion, magnetic sulfonated chitosan crosslinked with glutaraldehyde is a highly effective solution for mercury remediation in practical applications.

Keywords: Chitosan, Crosslinking, Hg, Regeneration, Isotherm

1. Introduction

Artisanal gold mining and poorly regulated anthropogenic activities often lead to increased environmental heavy metal pollution through wastewater discharge. This issue is particularly prevalent in rapidly developing economies like Indonesia, where artisanal gold mining has caused significant mercury contamination in aquatic ecosystems due to the amalgamation process and inadequate wastewater treatment. Direct exposure to mercury and its accumulation in the food chain can severely impact the local communities' quality of life [1]. Mercury is highly toxic even at low concentrations, posing serious health risks to both humans and wildlife. Hg^{2+} is particularly challenging to remove due to its complex chemical behavior, including its ability to form stable complexes with various organic and inorganic ligands [2]. Improving wastewater treatment and remediating mercury-contaminated environments are critical steps in mitigating these impacts. Chitosan, a biopolymer derived from fungi or crustaceans, offers significant potential as an adsorbent for mercury removal from water. It is biodegradable, non-toxic, and highly modifiable, making it an environmentally friendly option [3]. Chitosan contains key functional groups, such as O- and N-containing moieties, that

Received 27 November 2024; revised 9 March 2025; accepted 11 March 2025.
Available online 5 April 2025

* Corresponding author.
E-mail address: rahmi@usk.ac.id (Rahmi).

https://doi.org/10.33640/2405-609X.3401

can serve as binding sites for mercury uptake. These groups interact with metal cations through electrostatic forces and complexation, enhancing their effectiveness as an adsorbent.

Functional groups in an adsorbent play a crucial role in attracting adsorbates, facilitating their diffusion into the solid phase. Beyond well-known functional groups, S-containing groups have been shown to enhance heavy metal uptake. For instance, a previous study demonstrated improved Hg^{2+} adsorption by incorporating S-functional groups into biochar via plasma modification [4]. Another study reported a 50 % removal of heavy metals via complexation with sulfonate groups in a chitosan-based flocculant containing S-functional groups [5]. Sulfonate groups (SO_3^-), as S-containing functional groups, can form covalent bonds with metal ions, either as S-metal or O-metal complexes [6]. X-ray photoelectron spectroscopy analysis has revealed that functional groups such as C═O or O-C═O significantly contribute to mercury uptake, whereas C-O (from O-H) does not [4]. Additionally, O-containing functional groups can act as electron acceptors, oxidizing Hg^0 to Hg^{2+}, thereby enhancing adsorption since Hg^{2+} is more favorable for electrostatic interactions [7]. This study aims to modify chitosan by replacing its hydroxyl functional groups (O-H) with sulfonate groups using a sulfonating agent. This approach incorporates S-containing functional groups to improve mercury adsorption capacity.

In previous studies, various materials have been applied for water treatment such as carbon-based sorbents [8], hydrocar [9], carboxymethylcellulose-iron composite [10], activated carbon [11], zinc oxide marigold [12], MWCNTs/ThO2 nanocomposite [13], CNTs [14], silico-manganese fumes waste encapsulated cryogenic alginate beads [15], and cross-linked chitosan-activated charcoal [16]. While these adsorbents exhibit high adsorption capacities, challenges such as complex synthesis procedures and high production costs remain. Therefore, developing a magnetic sulfonated chitosan adsorbent that offers a simpler synthesis process, lower production costs, and minimal environmental impact is crucial to address these limitations and provide a more sustainable solution for water treatment applications.

The use of the sulfonating agent $N(SO_3Na)_3$, derived from a reaction between $NaNO_2$ and $NaHSO_3$, in this study was inspired by previous study [17]. This agent reacts with hydroxyl groups in chitosan, replacing -OH with -OSO_2Na (Fig. 1). While sulfonation of chitosan is not new, previous studies have employed various sulfonating agents, such as sulfuric acid [18], 4-formyl-1,3-benzene disulfonate [19], and 1,3-propane sulfone [20]. In this study, glutaraldehyde was also used as a crosslinking agent to improve the material's performance in aqueous mercury removal. Crosslinking enhances the durability of chitosan, which is prone to dissolution in acidic solutions and structural rupture during application [21–23]. Glutaraldehyde achieves this by reacting with amino groups ($-NH_2$) in chitosan to form stable imine bonds (Schiff bases). Our research group has previously used different crosslinking agents such as H_2SO_4, poly(ethylene glycol) diglycidyl ether, and epichlorohydrin, demonstrating their positive effects on the adsorptive removal of aqueous pollutants. In this study, the sulfonation process using $N(SO_3Na)_3$ consumes hydroxyl groups (O-H), requiring the crosslinking reaction to target amino groups (N-H). Consequently, glutaraldehyde was selected as the crosslinking agent (Fig. 1). We hypothesized that the introduction of the -OSO_2Na moiety would increase the number of active sites on the adsorbent surface, enhancing pollutant uptake. Additionally, crosslinking with glutaraldehyde was expected to yield a material with improved properties, including greater regenerability. A previous study used glutaraldehyde to crosslink sulfonated chitosan for organic dye (methylene blue) removal, employing a different sulfonating agent (4-formyl-1,3-benzene disulfonate) via hydrothermal grafting [19]. In the present study, however, we synthesized the adsorbent in bead form, embedded it with magnetic iron sand (IS), and applied it for mercury removal. This study also demonstrated the applicability of the IS/$NaSO_3$-Chi-G bead composite for real mercury-contaminated water and evaluated its regeneration capability.

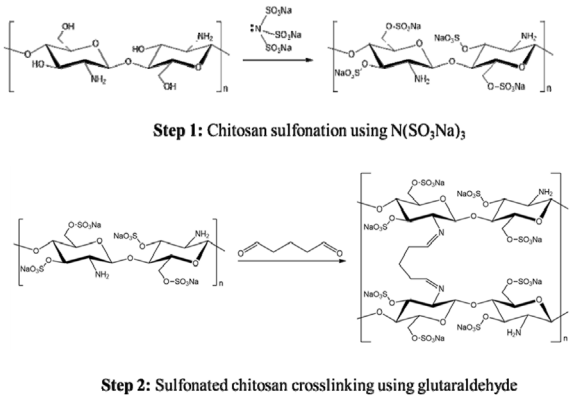

Fig. 1. Schematic diagram of two-step reactions in synthesizing sulfonated chitosan crosslinked with glutaraldehyde.

2. Materials and methods

2.1. Materials

The chemicals used in this study, including glacial acetic acid (99.5 % purity), ammonium hydroxide (NH_4OH; 99.9 % purity), nitric acid (HNO_3; 68 % purity), hydrochloric acid (HCl; 37 % purity), sodium hydroxide (NaOH; 98.5 % purity), sulfuric acid (H_2SO_4; 98 % purity), sodium nitrite ($NaNO_2$; 99.9 % purity), sodium bisulfite ($NaHSO_3$; 58.5 %), and glutaraldehyde (25 % aqueous solution), were all of analytical grade and procured from Merck (Selangor, Malaysia). The primary polymer, high-molecular-weight chitosan with a deacetylation degree of 75.0 % to 85.0 %, was obtained from Tokyo Chemical Industry (Tokyo, Japan). Iron sand (IS) was extracted from beach sand collected at Syiah Kuala Beach, Banda Aceh, Indonesia, using a magnet. The IS was thoroughly washed with boiling deionized water and then oven-dried at 70 °C for 24 h. Following this, the dried IS was ball-milled for 20 min at 300 rpm. The sulfonating agent, $N(SO_3Na)_3$, was synthesized by mixing solutions of $NaNO_2$ and $NaHSO_3$ in a 1:4.25 volume ratio in a beaker at 90 °C and 250 rpm for 90 min. This method was adapted from a previously published procedure [17].

Mercury-contaminated water was collected on March 5, 2019, from the Manggamat River in Aceh Selatan Regency, Aceh Province, Indonesia (3.1873°N, 97.3895°E). Sampling locations were near artisanal gold mining sites where mercury was used in the amalgamation process. Initial mercury concentrations from six sampling points were measured as 0.675, 0.537, 0.468, 0.843, 0.211, and 0.264 mg/L, respectively. The water samples were stored in polyethylene bottles, labeled, and immediately acidified with 2 N HNO_3 before transportation to the laboratory.

2.2. Iron sand/$NaSO_3$-Chi-G composite preparation

For sulfonation, chitosan flakes were soaked in the freshly prepared sulfonating agent, $N(SO_3Na)_3$, with a pH of 5, and left for 24 h at 27°C ± 2 °C. The sulfonated chitosan was then collected by filtration, rinsed with deionized water, and oven-dried at 40 °C for 7 h. To produce a chitosan film, the sulfonated chitosan was dissolved in 20 mL of 2 % glacial acetic acid and stirred for 2 h at room temperature. Subsequently, 0.5 g of iron sand was added to the solution and stirred for an additional hour. The weight of dissolved chitosan was varied (0.35, 0.4, 0.45, 0.5, 0.55, 0.6, and 0.65 g), resulting in iron sand ratios of 58.8 %, 55.6, 52.6, 50, 47.6, 45.5, and 43.5 % w/w, respectively. The casting solution was transferred into a syringe and added dropwise into a 250 mL NaOH (3 M) solution. The formed beads were washed with deionized water until the pH reached 7, then oven-dried at 40 °C for 12 h. The resulting sample was labeled as IS/$NaSO_3$-Chi.

For the crosslinked composite, the same protocol used for preparing IS/$NaSO_3$-Chi was followed. However, before adding the iron sand, glutaraldehyde at varying concentrations (0.04, 0.08, 0.13, 0.17, and 0.21 M) was added to the chitosan solution and stirred for 2 h. The resulting bead samples from this process were labeled as IS/$NaSO_3$-Chi-G.

2.3. Characterization

The observed characteristics included morphology, functional groups, and crystallinity. Morphology was examined using a Scanning Electron Microscope (SEM, Jeol JSM-6510 LA, Tokyo, Japan) at a maximum magnification of 30,000× and an operating voltage of 15 kV. Functional groups of neat chitosan, iron sand, IS/$NaSO_3$-Chi, and IS/$NaSO_3$-Chi-G were analyzed using a Shimadzu Fourier Transform Infrared (FT-IR) spectrometer (Kyoto, Japan). Crystallinity was assessed with a Shimadzu X-Ray Diffractometer (XRD-700, Kyoto, Japan), and the crystallinity index was calculated using a peak-to-noise ratio formula. Data processing included a smoothing procedure with the Savitzky-Golay method, applying a 50-point window in OriginPro 2021 (version 9.8.0.200, Northampton, MA, USA). All samples subjected to FT-IR and XRD characterization were pre-dried overnight at 40 °C.

2.4. Batch adsorption

To determine the optimal compositions of iron sand and glutaraldehyde, as well as adsorption parameters, an artificial mercury-contaminated solution was prepared using $HgCl_2$ dissolved in distilled water. The solution volume and adsorbent mass were fixed at 10 mL and 0.1 g, respectively, for all experiments. For optimizing the compositions of iron sand and glutaraldehyde, 0.1 g of adsorbent was used with an initial mercury concentration of 300 mg/L at pH 7. To investigate the effect of contact time, experiments were conducted with contact durations ranging from 5 to 100 min at pH 7 and an initial mercury concentration of 300 mg/L. The influence of pH on mercury removal was evaluated at the optimal contact time (60 min), with pH levels varied between 2 and 9.

All batch adsorption experiments were carried out in Erlenmeyer flasks placed on a rotary shaker

operating at 250 rpm at room temperature. After each experiment, the adsorbent was separated using a magnet attached to the outside of the flask. The remaining mercury concentration in the water was measured using a Shimadzu AA-6300 Atomic Absorption Spectrophotometer (Kyoto, Japan). The same procedure was applied to a real mercury-contaminated water sample collected earlier for comparison. Each batch adsorption experiment was performed in triplicate to ensure reproducibility.

2.5. Regeneration

After each adsorption batch, the composite beads (0.1 g) were soaked in 250 mL of 3 M H_2SO_4 for 30 min at 250 rpm and room temperature. The beads were then removed from the acid solution and thoroughly washed with deionized water until the surface pH reached neutral (pH 7). Subsequently, the beads were oven-dried at 40 °C for 12 h. The dried composite beads were reused for the next cycle of batch adsorption, with an initial mercury concentration of 300 mg/L for each cycle. The same batch adsorption conditions were maintained across all regeneration cycles to ensure consistency. Large-scale treatment of contaminated water was conducted by previous study with different removal procedures for some heavy metal ions [24].

3. Results and discussions

3.1. Characteristics of IS/SO_3-Chi-G composite

The surface morphology of ball-milled iron sand was analyzed using SEM at 1,000× and 30,000× magnifications (Fig. 2a). The particle size was heterogeneous, ranging from approximately 0.1 to 0.3 μm, with irregular shapes. SEM images of chitosan beads at 100× magnification revealed a spheroidal shape with a smooth surface (Fig. 2b). However, at 30,000× magnification, the surface appeared rough and wavy. The embedment of iron sand onto sulfonated chitosan (IS/$NaSO_3$-Chi) resulted in the bead surface being covered with irregularly shaped small particles, identified as iron sand (Fig. 2c). Similar particles were also observed covering the surface of IS/$NaSO_3$-Chi-G beads (Fig. 2d).

The effect of crosslinking on the surface morphology of IS/$NaSO_3$-Chi-G beads was also observed. Following crosslinking, agglomerations were evident under SEM analysis and were attributed to non-crosslinked chitosan regions. Glutaraldehyde-crosslinked chitosan molecules exhibit a more rigid molecular structure, leading to a difference in density compared to non-crosslinked chitosan.

This density variation may result in agglomeration, as chitosan molecules can still form intermolecular bonds through amine groups. A similar phenomenon was noted in our previous study on polyol particles crosslinked with urethane linkages. Other researchers have also reported comparable morphological changes. For example, chitosan crosslinked with palladium (II) phthalocyanine tetrasulfonate via amine groups showed similar agglomeration, although no explanation was provided for this observation [25]. Romal and Ong also described changes in morphology after crosslinking, offering explanations in their study [26]. Furthermore, in another work, they observed morphological alterations when phosphorylating the C6-OH of chitosan, even without a crosslinker [27]. In summary, the morphology of IS/$NaSO_3$-Chi-G appears rough with agglomerated chitosan regions, which may be associated with its mercury uptake capability.

The FT-IR spectra of chitosan, IS/$NaSO_3$-Chi, and IS/$NaSO_3$-Chi-G composites are presented in Fig. 3. The absorption band in the range of 3700–3000 cm^{-1} corresponds to O-H stretching and N-H stretching vibrations of primary amines [28]. Shifts in spectral signals and variations in the amide I band (1700–1600 cm^{-1}) and amide II band (near 1550 cm^{-1}) were observed, indicating interactions with metal ions [29]. The medium-intensity bands at 1654.92 cm^{-1} (a) and 1633.71 cm^{-1} (c, d) are attributed to the vibrational region of amide I (C═O stretching) [30].

Additionally, a shift in the weak to medium-intensity bands from 1587.42 cm^{-1} (c) to 1585.49 cm^{-1} (d) is associated with C-N stretching coupled with N-H bending. This confirms the formation of a bond between NH_2 and the aldehyde group (C═O) of glutaraldehyde, forming amide II and validating successful glutaraldehyde crosslinking in the chitosan. The band at 1375 cm^{-1} represents CH_2 scissoring vibrations, while the peak at 1070 cm^{-1} corresponds to S═O stretching, indicative of sulfonic acid groups. However, this does not specify whether sulfonation occurred at both the C3 and C6 positions or only at C6. New functional groups were identified in the spectra of IS/$NaSO_3$-Chi and IS/$NaSO_3$-Chi-G. The band at 896.90 cm^{-1} represents C-O-S bond vibrations from sulfonation, and the band at 578.64 cm^{-1} corresponds to Fe-O bond vibrations from the iron sand. These findings confirm the successful incorporation of sulfonic and iron sand groups into the composites.

The crystallographic structures of iron sand, chitosan, $NaSO_3$-Chi, and IS/$NaSO_3$-Chi-G were analyzed using XRD, and the results are presented

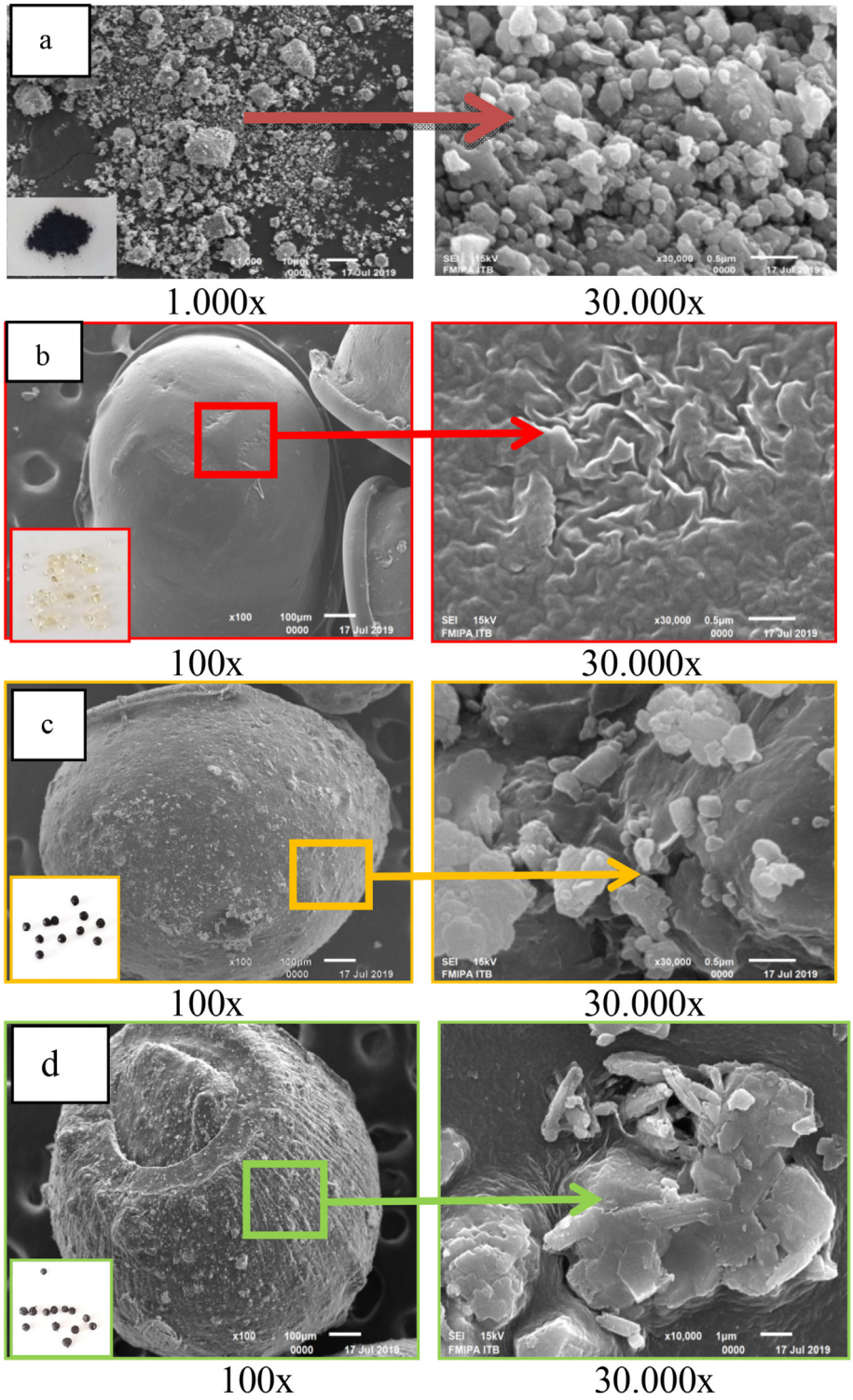

Fig. 2. Surface morphology of iron sand particles resulted from the ball-milling process observed under 1,000× (left) and 30,000× (right) magnifications (a). Surface morphologies of chitosan (b), IS/$NaSO_3$-Chi (c), and IS/$NaSO_3$-Chi-G (d) beads were observed under 100× (left) and 30,000× (right).

in Fig. 4. The diffractogram of iron sand nanoparticles exhibits peaks at 2θ values of 30.13°, 35.50°, 43.13°, 57.03°, and 62.63°, which are characteristic of Fe_3O_4. These peaks correspond to the (220), (311), (400), (511), and (440) planes, representing the crystalline cubic magnetite structure (JCPDS reference No. 01–075-0033) [46]. For chitosan (Fig. 4b), a broad peak at 2θ = 21.8° indicates its

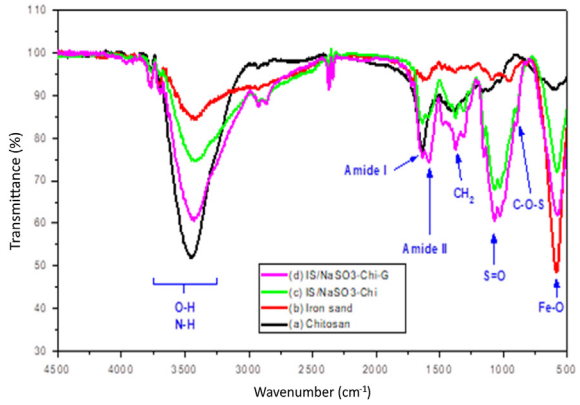

Fig. 3. FT-IR spectra of chitosan (a), iron sand (b), IS/$NaSO_3$-Chi (c), and IS/$NaSO_3$-Chi-G (d).

semi-crystalline nature [31,32]. In the IS/$NaSO_3$-Chi and IS/$NaSO_3$-Chi-G composite samples, distinct peaks at $2\theta = 35.8°$ and 36.01°, respectively, confirm the presence of Fe_3O_4 from the iron sand. However, the characteristic crystalline peak of chitosan is not observed in these composites, suggesting that the crystallinity of the iron sand dominates within the material. This observation aligns with previous studies on hydroxyapatite-embedded chitosan matrices, where the embedded component masked the chitosan crystallinity [33]. Overall, the XRD analysis confirms the successful incorporation of magnetic iron sand into the polymer matrix, as evidenced by the dominant crystalline peaks attributed to Fe_3O_4.

Regarding the crystallinity, we calculated the crystallinity index of each sample using the peak-to-noise ratio formula. Crystallinity indices of chitosan, IS/$NaSO_3$-Chi, and IS/$NaSO_3$-Chi-G samples were 78.15, 47.04, and 45.64, respectively. The crystallinity of chitosan dropped as much as 35.97 % when iron

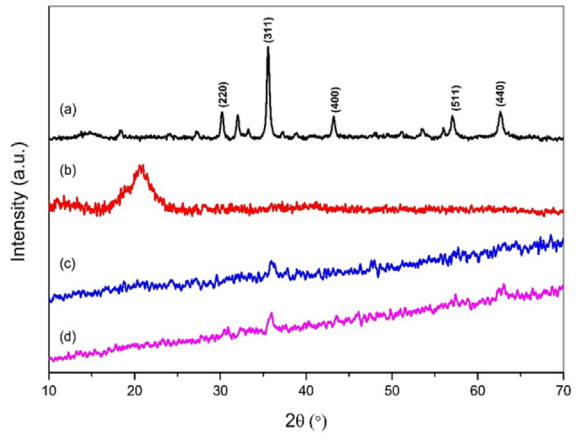

Fig. 4. XRD patterns of iron sand (a), chitosan (b), $NaSO_3$-Chi (c) and IS/$NaSO_3$-Chi-G (d).

sand fillers were introduced to the matrix. It also indicates the increase on the amorphousness of the prepared composites. Nonetheless, the crystallinity change was insignificantly observed between IS/$NaSO_3$-Chi and IS/$NaSO_3$-Chi-G, which is in agreement with the diffractogram shape. The findings of this research are in line with several previous studies where they reported significantly reduced crystallinity indices following the addition of Fe_3O_4 as filler particles [34].

3.2. Effect of iron sand filler on Hg^{2+} adsorption

The embedment of iron sand aimed to impart magnetic properties to the adsorbent, facilitating its easy separation from water after treatment. However, the addition of iron sand to the chitosan-based matrix influenced its adsorption capacity for Hg^{2+} (Fig. 5a). In the current study, the lowest Hg^{2+} adsorption capacity was observed with an iron sand composition of 58 % w/w in the chitosan matrix. Because high composition of iron sand reduced the chitosan content where chitosan is the main material for Hg^{2+} adsorption. Reducing the iron sand content to 55.6 % increased the adsorption capacity to 29.55 ± 0.03 mg/g. Further reductions in iron sand composition resulted in a gradual increase in Hg^{2+} adsorption capacity, with compositions of 52.6 %, 50 %, 47.6 %, and 45.5 % yielding capacities of 29.74 ± 0.02, 29.74 ± 0.04, 29.71 ± 0.05, and 29.75 ± 0.03 mg/g, respectively. The highest adsorption capacity for Hg^{2+} (30.74 ± 0.03 mg/g) was achieved with an iron sand composition of 43.5 % w/w in the chitosan-based adsorbent (Fig. 5a).

Similar findings were observed in a study using chitosan embedded with graphene oxide and nanocellulose, where the removal percentages of Pb and Cd fluctuated, as analyzed by inductively coupled plasma-optical emission spectrometry [35]. These variations in adsorption capacity can result from a tradeoff between the adsorptive benefits and disadvantages of filler addition. For IS/$NaSO_3$-Chi-G, fluctuations in adsorption capacity likely arise from this tradeoff. However, since the adsorbent with a 43.5 % iron sand composition achieved the highest Hg^{2+} adsorption capacity, it was selected for all subsequent experiments.

3.3. Effect of glutaraldehyde crosslinking on Hg^{2+} adsorption

The effect of glutaraldehyde concentration in IS/$NaSO_3$-Chi-G on Hg^{2+} removal is shown in Fig. 5b. An increase in adsorption capacity from 27.51 ± 0.12 mg/g to 28.23 ± 0.23 mg/g was observed

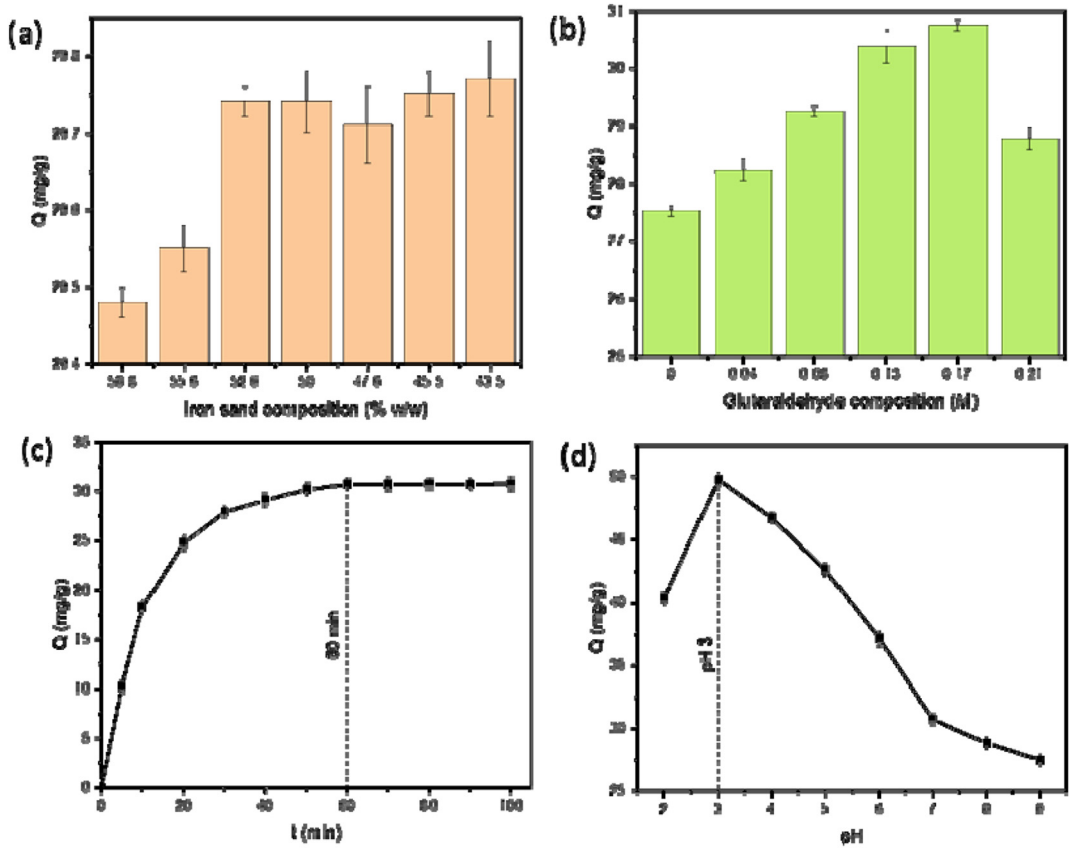

Fig. 5. Effect of iron sand filler (% w/w) (a) and crosslinking agent glutaraldehyde (M) (b) in the IS/$NaSO_3$-Chi-G composite on Hg^{2+} adsorption (t = 80 min; pH = 7). Effect of contact time variation (0—100 min) (c) and effect of pH variation (pH = 2—9) toward Hg^{2+} adsorption onto IS/$NaSO_3$-Chi-G composite. Otherwise stated, the adsorption parameters are as follows: adsorbent mass = 0.1 g; initial [Hg^{2+}] = 300 mg/L; 135 rpm; and room temperature. Dashed lines indicate an optimum contact time or pH.

when glutaraldehyde concentration was increased to 0.04 M during crosslinking. The adsorption capacity continued to rise with increasing glutaraldehyde concentration, reaching a peak of 30.74 ± 0.14 mg/g at 0.17 M. This trend highlights the positive correlation between glutaraldehyde-based crosslinking and the ability of IS/$NaSO_3$-Chi-G to adsorb Hg^{2+} from water. However, when the glutaraldehyde concentration was further increased to 0.21 M, the adsorption capacity declined to 28.78 ± 0.25 mg/g, indicating that excessive crosslinking may hinder adsorption efficiency.

Crosslinking with glutaraldehyde plays a critical role in pollutant adsorption by maintaining the structural integrity of chitosan in acidic or basic wastewater. This concept has also been highlighted in a study that used glutaraldehyde-crosslinked chitosan beads for Cr^{4+} removal [36]. In our previous research, we observed that chitosan tends to swell in acidic solutions, which enhances adsorbate diffusion and increases adsorption capacity. However, chitosan is inherently unstable in strongly acidic environments, leading to structural degradation of the adsorbent material. Glutaraldehyde crosslinking addresses these challenges by preventing the formation of an overly dense chitosan structure at basic pH levels and mitigating structural decay at acidic pH levels. However, in this study, we observed a reduction in adsorption capacity when the glutaraldehyde concentration was increased to 0.21 M. This decline can be attributed to over-crosslinking, which creates a denser and less porous chitosan structure. Over-crosslinking reduces the availability of active sites for Hg^{2+} adsorption, limits the diffusion of Hg^{2+} ions, and blocks functional groups, ultimately decreasing the overall adsorption capacity.

3.4. Batch adsorption parameter: contact time

The effect of contact time on Hg^{2+} adsorption was investigated over 100 min, and the results are presented in Fig. 5c. The adsorption capacity (Q) increased initially and reached equilibrium after 60 min (Q = 30.73 mg/g). Notably, previous research using neat Fe_3O_4 (iron sand) achieved a similar

adsorption capacity of about 28.8 mg/g but required 800 min [37]. In this study, the adsorption capacity rose sharply within the first 5 to 20 min, followed by a gradual increase until equilibrium was achieved. This behavior can be explained by the following rapid initial adsorption. During the early phase, the high Hg^{2+} concentration in the bulk solution drove rapid adsorbate diffusion onto the IS/$NaSO_3$-Chi-G composite. As the Hg^{2+} concentration in the solution decreased, the uptake rate slowed [38]. In later times, the adsorption rate decreased over time due to the progressive occupation of binding sites on IS/$NaSO_3$-Chi-G. As fewer binding sites remained available, the adsorption rate declined until all sites were occupied by Hg^{2+}. At equilibrium, the rates of adsorption and desorption became equal, resulting in no further changes in adsorption capacity [39]. These findings highlight the efficiency of IS/$NaSO_3$-Chi-G in rapidly adsorbing Hg^{2+} compared to pristine Fe_3O_4.

3.5. Adsorption batch parameter: pH

The effect of solution pH on Hg^{2+} adsorption by IS/$NaSO_3$-Chi-G was studied within the pH range of 2–9 (Fig. 5d). As the pH increased from 2 to 3, the adsorption capacity improved significantly, reaching 40.32 mg/g at pH 2 and peaking at 49.78 mg/g at pH 3. However, the adsorption capacity decreased as the pH increased further, dropping to a minimum of 27.5 mg/g at pH 9.

These changes can be explained by several factors, including surface charge, chitosan swelling, and the transformation of Hg^{2+} species in the solution. At lower pH levels, the amine groups in chitosan are protonated, imparting a more positive surface charge that can repel the cationic Hg^{2+} ions. However, the optimal adsorption at pH 3 suggests that glutaraldehyde crosslinking effectively consumes a significant portion of the amine groups, reducing this repulsion and allowing better interaction with Hg^{2+}. In acidic solutions, chitosan is prone to swelling, which increases the accessibility of binding sites for Hg^{2+}. This swelling mechanism contributes to the high adsorption capacity observed at pH 3. At higher pH levels, reduced swelling limits the availability of these binding sites. At higher pH levels, however, the Na^+ ions from the sulfonate (-$NaSO_3$) group may act as competitors, reducing the interaction of Hg^{2+} with the adsorbent [40]. Additionally, at basic pH, Hg^{2+} can react with hydroxyl (OH^-) ions to form insoluble complexes, resulting in precipitation and a further reduction in adsorption capacity [41]. Notably, the adsorption capacity sharply decreased from pH 3 to 7 and then declined slightly at pH 9. This trend underscores the importance of maintaining an optimal pH for effective Hg^{2+} removal, with pH 3 being identified as the most favorable condition.

The prepared IS/$NaSO_3$-Chi-G composite exhibits enhanced electrostatic advantages due to the sulfonate group, which dissociates into anionic SO_3^- in aqueous solution. This contributes to a more negatively charged adsorbent surface, facilitating higher Hg^{2+} adsorption [38]. While at acidic pH levels, the presence of H_3O^+ ions can compete with cationic Hg^{2+} for binding sites (as observed at pH 2), this competition diminishes at pH 3, where optimal adsorption was achieved. Comparing the adsorption capacities at acidic and basic pH ranges reveals significantly higher capacities in acidic conditions. This suggests that Hg^{2+} uptake by IS/$NaSO_3$-Chi-G is not predominantly driven by electrostatic interactions but is more likely influenced by swelling of the chitosan matrix and Hg^{2+} speciation.

The dominant interaction between adsorbate and adsorbent is proposed to occur via complex formation, either with the N ligand from glutaraldehyde [42] or the S=O ligand from the sulfonate group [6]. An illustration of the proposed adsorbate-adsorbent interaction mechanisms in this study is presented in Fig. 6.

3.6. Isotherm modeling

Herein, the adsorption of Hg^{2+} onto IS/$NaSO_3$-Chi-G was modeled using two widely applied isotherm models: Langmuir and Freundlich. The Langmuir model assumes homogeneous binding energies on the adsorbent surface and describes monolayer adsorption, where each binding site interacts equally with the adsorbate. In contrast, the Freundlich model is based on the assumption of heterogeneous binding energies across the

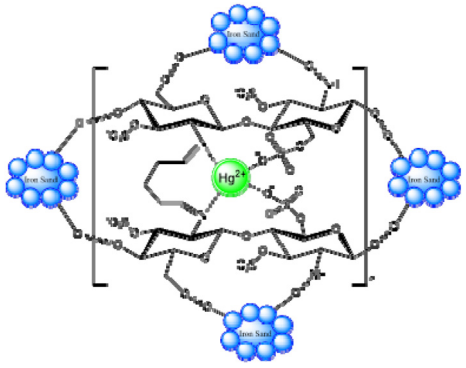

Fig. 6. Illustration of covalent bonding mechanism between IS/$NaSO_3$-Chi-G and Hg^{2+}. Dashed lines represent the covalent bond.

adsorbent surface and describes multilayer adsorption. The mathematical expressions for the Langmuir and Freundlich isotherm models are presented in Equations (1) and (2).

$$\frac{1}{Qe} = \left[\frac{1}{Q_m K_L}\right] \frac{1}{C_e} + \frac{1}{Q_m} \quad (1)$$

$$\log_{10} Qe = \log_{10} K_F + \frac{1}{n} \log_{10} C_e \quad (2)$$

where Q_e (mg/g), is the amount of Hg^{2+} adsorbed onto IS/$NaSO_3$-Chi-G, Q_m (mg/g) is the maximum adsorption capacity of IS/$NaSO_3$-Chi-G, C_e (mg/L) is the equilibrium concentration of ion Hg, K_L (L/mg) and K_F [(mg/g)(mg/$L^{-1/n}$)] are Langmuir and Freundlich constant, 1/n is the heterogeneity factor [43,44].

Linear regression curves of the experimental data based on the Langmuir and Freundlich isotherm models, along with their respective parameters, are shown in Table 1. The agreement between the predicted and experimental data was evaluated using the R^2 value. The R^2 value for the Freundlich model was higher, indicating that the interaction between Hg^{2+} and IS/$NaSO_3$-Chi-G is best explained by multilayer adsorption with heterogeneous binding energies [43].

Table 1. Langmuir and Freundlich Isotherm parameters for Hg^{2+} adsorption by IS/$NaSO_3$-Chi-G.

Langmuir Isotherm	
Q_m (mg/g)	93.46
K_L	0.57
R^2	0.97
RMSE	0.002
Freundlich isotherm	
K_F	32.99
N	2.08
R^2	0.98
RMSE	0.035

Table 2. Adsorption kinetic parameters of PFO and PSO kinetic models for Hg^{2+} adsorption by IS/$NaSO_3$-Chi-G.

Parameter	PFO	PSO
q_e	2.68 mg/g	370.37 mg/g
k	0.002 mg/g/min	0.0009 mg/g/min
R^2	0.8625	0.9999

The adsorptive behavior is likely due to the ability of the sulfonate groups to form covalent bonds with heavy metal ions. The Freundlich model's adsorption intensity constant (*n*) was greater than 1, suggesting that IS/$NaSO_3$-Chi-G is favorable for Hg^{2+} adsorption [45]. Additionally, the Langmuir isotherm also showed good applicability, with an R^2 value > 0.95, indicating that monolayer adsorption also contributes to the system. The maximum adsorption capacity (*Qm*) derived from the Langmuir model was 93.46 mg/g. This value is comparable to, and in some cases higher than, the capacities reported in other studies, as summarized in Table 3, highlighting the effectiveness of IS/$NaSO_3$-Chi-G for mercury removal.

3.7. Kinetic study

Pseudo-first-order (PFO) and pseudo-second-order (PSO) models were used to assess the adsorption kinetics. Table 2 shows the parameters derived from these models. According to the PFO kinetic model, physical adsorption governs the majority of the adsorption process, with the adsorption rate being proportional to the number of vacant adsorption sites. Systems where the adsorption process is dominated by van der Waals forces or other weak interactions are usually described using this model. The PSO kinetic model, on the other hand, indicates that chemical adsorption which includes valence forces and potentially the creation of surface coordination bonds between the adsorbent and the adsorbate controls the adsorption process. Higher correlation coefficients (R^2), which show a better fit of the experimental data to the PSO model, suggest that chemisorption processes were primarily responsible for Hg^{2+} adsorption by IS/$NaSO_3$-Chi-G. Metal ions adhere to the adsorbent's surface during chemisorption to create coordinated covalent bonds.

Table 3. Comparison of regeneration cycles and adsorption capacity maximum (Qm) between this present work and previously published studies.

Sample	Year	Ref	Regeneration (cycles)	Qm (mg/g)
Iron sand/glutaraldehyde-crosslinked sulfonated chitosan	2024	This work	>5	93.46
SnO_2-crosslinked-chitosan nanocomposite	2022	[46]	4	21.05
Modified ion-imprinted chitosan	2022	[47]	5	315
Thiophene-chitosan hydrogel-trap	2020	[48]	3	18.71
Fibrous polymer-grafted chitosan	2016	[49]	3	4.88 ± 0.21
Chitosan coated Fe_3O_4 nanocomposites	2016	[50]	12	96
Biobased chitosan derivative	2021	[51]	Not reported	107
Chitosan oligosaccharide/silica nanoparticles hybrid porous gel	2021	[52]	Not reported	33.3

3.8. Regeneration of $NaSO_3$-Chi-G for aqueous Hg^{2+} removal

The re-generatability of an adsorbent is crucial for enhancing the cost efficiency and eco-friendliness of wastewater treatment processes. In this study, the regeneration of IS/$NaSO_3$-Chi-G was performed over five cycles (Fig. 7). The adsorption capacity for Hg^{2+} was initially 49.98 ± 0.06 mg/g and remained nearly unchanged at 49.82 ± 0.02 mg/g after the fifth cycle. This minimal reduction in adsorption capacity even after multiple regeneration cycles confirms the excellent re-generatability of IS/$NaSO_3$-Chi-G. Such durability highlights its potential as a sustainable and reusable material for mercury removal in wastewater treatment.

Previously, we observed poor re-generatability in polyethylene glycol diglycidyl ether-crosslinked chitosan, where the heavy metal adsorption capacity decreased dramatically after just one cycle. This issue was attributed to the degradation of functional groups, particularly amine groups, and/or an ineffective regeneration protocol. In this study, we employed a similar regeneration protocol using 3 M H_2SO_4 to desorb mercury from IS/$NaSO_3$-Chi-G. Thus, the primary factor influencing re-generatability is likely the preservation of functional groups during regeneration cycles.

In the present study, the degradation of key functional groups was effectively minimized, likely due to glutaraldehyde crosslinking, which enhances chitosan's stability in acidic conditions [72]. It was confirmed by the existence of typical absorption bands of chitosan, iron sand, and sulfonate groups in the FTIR spectrum of IS/$NaSO_3$-Chi-G after 5 cycles of regeneration (Fig. 8).

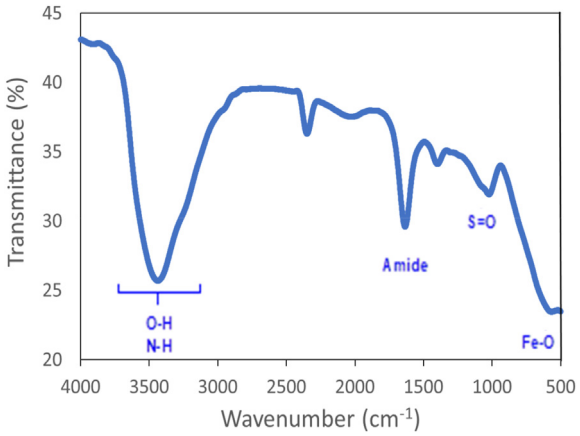

Fig. 8. FT-IR spectrum of IS/$NaSO_3$-Chi-G after 5 cycles of regeneration.

This improved stability allowed the IS/$NaSO_3$-Chi-G to maintain high adsorption capacity over multiple regeneration cycles. A comparison of the number of successful regeneration cycles achieved in this study with those reported in previously published works is presented in Table 2.

3.9. IS/NaSO3-Chi-G for remediating Hg-contaminated water

The performance of IS/$NaSO_3$-Chi-G in removing Hg from real water samples is presented in Fig. 9. The adsorptive efficiency observed in actual water samples may deviate from the results obtained in controlled laboratory conditions. This is partly because the isotherm study was conducted using a high range of Hg concentrations (300–800 mg/L), which may not fully represent real-world conditions. Despite this, a significant reduction in Hg

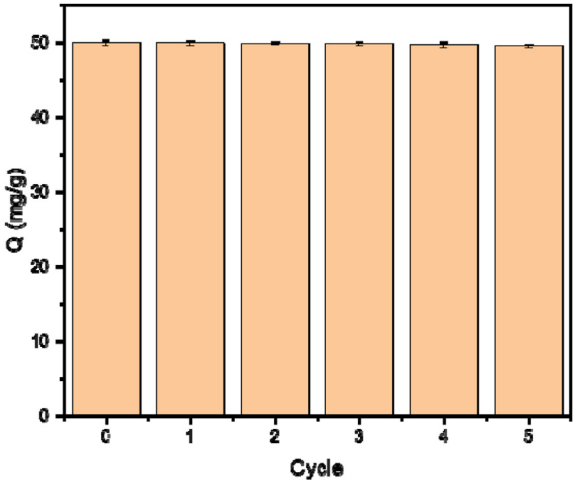

Fig. 7. Adsorption capacity of IS/$NaSO_3$-Chi-G for Hg^{2+} following 5 cycles of regeneration.

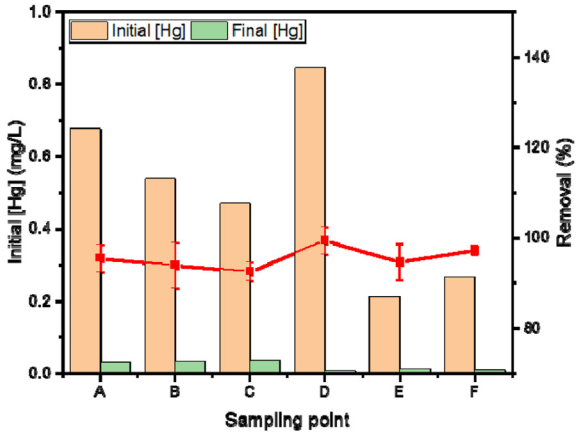

Fig. 9. Hg removal from the real sample using IS/$NaSO_3$-Chi-G. The red line indicates the removal percentage of Hg by IS/$NaSO_3$-Chi-G.

concentration was achieved following batch adsorption treatment with IS/$NaSO_3$-Chi-G, with nearly 100 % removal efficiency. The removal percentage appeared to correlate with the initial Hg concentration, likely due to the role of adsorbate concentration in driving diffusion forces. The variability in removal percentages could also be attributed to the presence of competing cationic ions in the water, which may interfere with adsorption. Additionally, Hg in real water samples may exist in various forms—organic or inorganic—and in different oxidation states (e.g., Hg^0, Hg^+, and Hg^{2+}). Nevertheless, the results confirm the high efficacy of IS/$NaSO_3$-Chi-G composite beads in removing mercury from real contaminated water samples, demonstrating their potential for practical applications.

4. Conclusions

The IS/$NaSO_3$-Chi-G composite beads were successfully synthesized through a two-step reaction involving sulfonation with $N(SO_3Na)_3$ and cross-linking with glutaraldehyde. The modification introduced a new functional group, SO_3Na, as confirmed by FT-IR analysis. Additionally, the combination of sulfonation and the incorporation of magnetic iron sand led to changes in crystallinity and surface morphology. The optimal conditions for Hg^{2+} adsorption onto IS/$NaSO_3$-Chi-G composite beads were determined to be a contact time of 60 min and a pH of 3. Isotherm studies demonstrated the compatibility of both Langmuir and Freundlich models, with the adsorption system aligning more closely with the Freundlich model. The material exhibited high regenerability, retaining its performance for more than five cycles of regeneration using a strong acid solution. Moreover, the adsorbent effectively removed mercury from real contaminated water samples, demonstrating its practical applicability. In conclusion, IS/$NaSO_3$-Chi-G composite beads present a promising solution for the remediation of heavy metal pollution in aquatic environments, offering a cost-efficient and eco-friendly approach.

Ethics information

This study did not involve human participants or animals, and ethical approval was not required according to the institutional and national guidelines.

Conflict of interest

The authors declare that they have no competing interests.

Funding

The authors gratefully thank Universitas Syiah Kuala and the Ministry of Research, Technology, and Higher Education Indonesia which provided financial support through “Penelitian Dasar” scheme with contract number 81/UN11.2.1/PT.01.03/DRPM/2020.

References

[1] H.A. Spiller, Rethinking mercury: the role of sele-nium in the pathophysiology of mercury toxicity, Clin. Toxicol. 56 (2018) 313–326, https://doi.org/10.1080/15563650.2017.1400555.
[2] D. Teng, K. Mao, W. Ali, G. Xu, G. Huang, N.K. Ni-azi, X. Feng, H. Zhang, Describing the toxicity and sources and the remediation technologies for mer-cury-contaminated soil, RSC Adv. 10 (2020) 23221–23232, https://doi.org/10.1039/D0RA01507E.
[3] G.d.V. Brião, J.R.d. Andrade, M.G. C.d. Silva, M.G.A. Vieira, Removal of toxic metals from water using chitosan-based magnetic adsorbents. A re-view, Environ. Chem. Lett. 18 (2020) 1145–1168, https://doi.org/10.1007/s10311-020-01003-y.
[4] H. Zhang, T. Wang, Z. Sui, Y. Zhang, B. Sun, W.P. Pan, Enhanced mercury removal by transplanting sulfur-containing functional groups to biochar through plasma, Fuel 253 (2019) 703–712, https://doi.org/10.1016/j.fuel.2019.05.068.
[5] X. Tang, T. Huang, S. Zhang, W. Wang, H. Zheng, The role of sulfonated chitosan-based flocculant in the treatment of hematite wastewater containing heavy metals, Colloids Surf. A Physicochem. Eng. Asp. 585 (2020) 124070, https://doi.org/10.1016/j.colsurfa.2019.124070.
[6] B.F. Abrahams, C.T. Abrahams, M.G. Haywood, T.A. Hudson, B. Moubaraki, K.S. Murray, R. Rob-son, 3d-Metal derivatives of the [Cu(I)(SO3)4]7- ion: structure and magnetism, Dalton Trans. 41 (2012) 4091–4099, https://doi.org/10.1039/C2DT12337A.
[7] Z. Tan, L. Sun, J. Xiang, H. Zeng, Z. Liu, S. Hu, J. Qiu, Gas-phase elemental mercury removal by nov-el carbon-based sorbents, Carbon 50 (2012) 362–371, https://doi.org/10.1016/j.carbon.2011.08.036.
[8] M.A. Suliman, M. Sajid, M.K. Nazal, M.A. Islam, Carbon-based materials as promising sorbents for analytical sample preparation: recent advances and trends in extraction of toxic metal pollutants from various media, TrAC, Trends Anal. Chem. 167 (2023) 117265, https://doi.org/10.1016/j.trac.2023.117265.
[9] A.A. Alqadami, S.M. Wabaidur, B.H. Jeon, M.A. Khan, Co-hydrothermal valorization of food waste: process optimization, characterization, and water decolorization application, Biomass Conv. Bioref. 14 (2024) 15757–15768, https://doi.org/10.1007/s13399-022-03711-7.
[10] I. Ali, O.M.L. Alharbi, Z.A. Alothman, A. Al-warthan, A.M. Al-Mohaimeed, Preparation of a carboxymethylcellulose-iron composite for uptake of atorvastatin in water, Int. J. Biol. Macromol. 132 (2019) 244–253, https://doi.org/10.1016/j.ijbiomac.2019.03.211.
[11] V.S. Sivasankarapillai, S. Baskaran, A. Sundarara-jan, M.R. Siddiqui, S.M. Wabaidur, A. Muthuk-rishnan, R. Dhanusuraman, Porous network of ni-trogen self-doped honeycomb like activated carbon derived from Caladium tricolor leaves: a multifunc-tional platform for energy and environmental ap-plications, J. Porous Mater. 31 (2024) 1489–1502, https://doi.org/10.1007/s10934-024-01580-1.
[12] N. Ansari, A. Ali, M.S. Akhtar, S. Hasan, T. Kha-toon, A.R. Khan, S.M. Wabaidur, Q.I. Rahman, Green synthesis of zinc oxide marigold shaped clus-ters using Eucalyptus globulus leaf extract as robust photocatalyst for dyes degradation under sunlight, Mater. Sci. Semicond. Process. 173 (2024) 108087, https://doi.org/10.1016/j.mssp.2023.108087.

[13] A. Mittal, M. Naushad, G. Sharma, Z.A. Alo-thman, S.M. Wabaidur, M. Alam, Fabrication of MWCNTs/ThO2 nano-composite and its adsorption behavior for the removal of Pb(II) metal from aqueous medium, Desalinat Water Treat-ment 57 (2015) 21863–21869, https://doi.org/10.1080/19443994.2015.1125805.
[14] I. Ali, M.L. Omar, Z.A. Alharbi, Z.A. Alothman, A.M. Al-Mohaimeed, A. Alwarthan, Modeling of fenuron pesticide adsorption on CNTs for mecha-nistic insight and removal in water, Environ. Res. 170 (2019) 389–397, https://doi.org/10.1016/j.envres.2018.12.066.
[15] M.A. Khan, S.M. Wabaidur, M.R. Siddiqui, A.A. Alqadami, A.H. Khan, Silico-manganese fumes waste encapsulated cryogenic alginate beads for aqueous environment de-colorization, J. Clean. Prod. 244 (2020) 118867, https://doi.org/10.1016/j.jclepro.2019.118867.
[16] A.K. Shukla, J. Alam, S. Mallik, J. Ruokolainen, K.K. Kesari, M. Alhoshan, Optimization and prediction of dye adsorp-tion utilising cross-linked chi-tosan-activated charcoal: response Surface Meth-odology and machine learning, J. Mol. Liq. 411 (2024) 125745, https://doi.org/10.1016/j.molliq.2024.125745.
[17] T. Wang, Y. Zhou, W. Xie, L. Chen, H. Zheng, L. Fan, Preparation and anticoagulant activity of N-succinyl chitosan sulfates, Int. J. Biol. Macromol. 51 (2012) 808–814, https://doi.org/10.1016/j.ijbiomac.2012.07.029.
[18] X. Zhang, J. Sun, Synthesis, characterization, and pro-perties of sulfonated chitosan for protein ad-sorption, Int. J. Polym. Sci. 2020 (2020) 1–10, https://doi.org/10.1155/2020/9876408.
[19] S. Sabar, H. Abdul Aziz, N.H. Yusof, S. Subrama-niam, K.Y. Foo, L.D. Wilson, H.K. Lee, Preparation of sulfonated chito-san for enhanced adsorption of methylene blue from aqueous solution, React. Funct. Polym. 151 (2020) 104584, https://doi.org/10.1016/j.reactfunctpolym.2020.104584.
[20] Z. Sun, C. Shi, X. Wang, Q. Fang, J. Huang, Synthe-sis, characterization, and antimicrobial activities of sulfonated chitosan, Carbohydr. Polym. 155 (2017) 321–328, https://doi.org/10.1016/j.carbpol.2016.08.069.
[21] M.L. Pita-López, G. Fletes-Vargas, H. Espi-nosa-Andrews, R. Rodríguez-Rodríguez, Physically cross-linked chitosan-based hydrogels for tissue en-gineering applications: a state-of-the-art review, Eur. Polym. J. 145 (2021) 110176, https://doi.org/10.1016/j.eurpolymj.2020.110176.
[22] O.A.C. Monteiro, C. Airoldi, Some studies of cross-linking chitosan–glutaraldehyde interaction in a homogeneous system, Int. J. Biol. Macromol. 26 (1999) 119–128, https://doi.org/10.1016/S0141-8130(99)00068-9.
[23] A.A. Hamid, J. Alam, A.K. Shukla, F.A.A. Ali, M. Alhoshan, Sustainable removal of phenol from wastewater using a biopolymer hydrogel adsorbent comprising cross-linked chitosan and κ-carrageenan, Int. J. Biol. Macromol. 251 (2023) 126340, https://doi.org/10.1016/j.ijbiomac.2023.126340.
[24] Z.A. Alothman, A.H. Bahkali, M.A. Khiyami, S.M. Alfadul, S. M. Wabaidur, M. Alam, B.Z. Al-farhan, Low cost biosorbents from fungi for heavy metals removal from wastewater, Separ. Sci. Technol. 55 (2019) 1766–1775, https://doi.org/10.1080/01496395.2019.1608242.
[25] A. Al-Azmi, S. Keshipour, Cross-linked chitosan aerogel modified with Pd(II)/phthalocyanine: syn-thesis, character-ization, and catalytic application, Sci. Rep. 9 (2019) 13849, https://doi.org/10.1038/s41598-019-50021-6.
[26] J.R.A. Romal, S.K. Ong, Single-Step fabrication of a dual-sensitive chitosan hydrogel by mannich reac-tion: synthesis, physicochemical properties, and screening of its Cu2+ up-take, Processes 11 (2023) 354, https://doi.org/10.3390/pr11020354.
[27] J.R.A. Romal, S.K. Ong, Opportunity for a greener recovery of dysprosium (III) from secondary sources by a novel Mannich reaction-modified phosphorylated chitosan hydrogel, Intern Int. J. Bi-ol. Macromol. 267 (2024) 131449, https://doi.org/10.1016/j.ijbiomac.2024.131449.
[28] A.M.A. El-Soad, M.O.A. El-Magied, M.S. Atrees, E.G. Kovaleva, G. Lazzara, Synthesis and charac-terization of modified sulfonated chitosan for beryl-lium recovery, Int. J. Biol. Macromol. 139 (2019) 153–160, https://doi.org/10.1016/j.ijbiomac.2019.07.162.
[29] H. Alhazmi, FT-IR spectroscopy for the identifica-tion of binding sites and measurements of the binding interactions of important metal ions with bovine serum albumin, Sci. Pharm. 87 (2019) 5, https://doi.org/10.3390/scipharm87010005.
[30] E. Kenawy, A.A. Ghfar, S.M. Wabaidur, M.A. Khan, M.R. Siddiqui, Z.A. Alothman, A.A. Alqadami, M. Hamid, Cetyl-trimethylammonium bromide intercalated and branched polyhy-droxystyrene functionalized montmorillonite clay to sequester cationic dyes, J. Environ. Manag. 219 (2018) 285–293, https://doi.org/10.1016/j.jenvman.2018.04.121.
[31] D. Malwal, P. Gopinath, Silica stabilized magnet-ic-chitosan beads for removal of arsenic from water, Colloids Interface Sci. Commun. 19 (2017) 14–19, https://doi.org/10.1016/j.colcom.2017.06.003.
[32] R.K. Shah, A.M. Naglah, Nanoarchitectonics of chitosan/glutaraldehyde/zinc oxide as a novel composite for the effi-cient removal of eriochrome black T dye from aqueous media, J. Inorg. Or-ganomet. Polym. Mater. 32 (2022) 2030–2039, https://doi.org/10.1007/s10904-022-02258-4.
[33] R.P. Alanis-Gomez, E.M. Rivera-Munoz, G. Lu-na-Barcenas, J.R. Alanis-Gomez, R. Ve-lazquez-Castillo, Improving the mechanical Re-sistance of hydroxyapatite/chitosan composite materials made of nanofibers with crystalline pref-erential orientation, Materials 15 (2022) 4718, https://doi.org/10.3390/ma15134718.
[34] M. Ahmadi, M. Pourmadadi, S.A. Ghorbanian, F. Yazdian, H. Rashedi, Ultra pH-sensitive nanocarrier based on Fe2O3/chitosan/montmorillonite for quer-cetin delivery, Int. J. Biol. Macromol. 191 (2021) 738–745, https://doi.org/10.1016/j.ijbiomac.2021.09.023.
[35] K. Ozge, C. Hande, Chitosan/graphene ox-ide/nanocellulose composites for removal of Cu(II) and Pb(II) ions in aqueous solution, Polym. Sci. A. 63 (2021) 556–567, https://doi.org/10.1134/S0965545X21050084.
[36] V. Watwe, P. Kulkarni, Evaluation of Cr(VI) adsorp-tion on glutaraldehyde crosslinked chitosan beads using cyclic voltammetry employing gold electrode, J. Anal. Sci. Tech-nol. 12 (2021) 37, https://doi.org/10.1186/s40543-021-00291-5.
[37] V.J. Inglezakis, A. Kurbanova, A. Molkenova, A.A. Zorpas, T. S. Atabaev, Magnetic Fe3O4-Ag0 Nano-Composites for Effective Mercury Removal from Water, Sustaina-bility 12 (2020) 5489, https://doi.org/10.3390/su12135489.
[38] P. Sricharoen, N. Limchoowong, P. Nuengmatcha, S. Chanthai, Ultrasonic-assisted recycling of Nile ti-lapia fish scale biowaste into low-cost nano-hydroxyapatite: ultra-sonic-assisted adsorp-tion for Hg2+ removal from aqueous solution fol-lowed by "turn-off" fluorescent sensor based on Hg2+-graphene quantum dots, Ultrason. Sonochem. 63 (2020) 104966, https://doi.org/10.1016/j.ultsonch.2020.104966.
[39] M. Hadavifar, N. Bahramifar, H. Younesi, M. Rastakhiz, Q. Li, J. Yu, E. Eftekhari, Removal of mercury (II) and cadmium (II) ions from synthetic wastewater by a newly synthesized amino and thi-olated multi-walled carbon nano-tubes, J. Taiwan Inst. Chem. Eng. 67 (2016) 397–405, https://doi.org/10.1016/j.jtice.2016.08.029.
[40] N. Nematidil, M. Sadeghi, S. Nezami, H. Sadeghi, Synthe-sis and characterization of Schiff-base based chi-tosan-g-glutaraldehyde/NaMMTNPs-APTES for removal Pb2+ and Hg2+ ions, Carbohydr. Polym. 222 (2019) 114971, https://doi.org/10.1016/j.carbpol.2019.114971.
[41] M. Alimohammady, M. Ghaemi, Adsorptive re-moval of Hg2+ from aqueous solutions using amino phenyl-pyrazole-functionalized graphene oxide, Carbon Lett. 30 (2020) 493–508, https://doi.org/10.1007/s42823-019-00119-8.
[42] M. Chen, M. Yu, R. Kang, H. Sun, W. Zhang, S. Wang, N. Wang, J. Wang, Removal of Pb (II) and V (V) from aqueous solution by glutaraldehyde cross-linked chitosan and

nanocomposites, Chemosphere 297 (2022) 134084, https://doi.org/10.1016/j.chemosphere.2022.134084.
[43] F. Ahmadijokani, H. Molavi, A. Peyghambari, A. Shojaei, M. Rezakazemi, T.M. Aminabhavi, M. Arjmand, Efficient removal of heavy metal ions from aqueous media by un-modified and modified nanodiamonds, J. Environ. Manag. 316 (2022) 115214, https://doi.org/10.1016/j.jenvman.2022.115214.
[44] V.T. Quyen, T.H. Pham, J. Kim, D.M. Thanh, P.Q. Thang, Q. Van Le, S.H. Jung, T. Kim, Biosorbent de-rived from coffee husk for efficient removal of tox-ic heavy metals from wastewater, Chemosphere 284 (2021) 131312, https://doi.org/10.1016/j.chemosphere.2021.131312.
[45] J. Galan, J. Trilleras, P.A. Zapata, V.A. Arana, C.D. Grande-Tovar, Optimization of chitosan glutaral-dehyde-crosslinked beads for reactive blue 4 an-ionic dye removal using a surface response methodology, Life 11 (2021) 85, https://doi.org/10.3390/life11020085.
[46] M.E. Mahmoud, M.S. Abdelwahab, G.A.A. Ibra-him, The design of SnO2-crosslinked-chitosan nanocomposite for microwave-assisted adsorption of aqueous cadmium and mercury ions, Sus. Chem. Pharm. 28 (2022) 100731, https://doi.org/10.1016/j.scp.2022.100731.
[47] A.K. Hajri, B. Jamoussi, A.E. Albalawi, O.H.N. Alhawiti, A.A. Alsharif, Designing of modified ion-imprinted chitosan particles for selective remov-al of mercury (II) ions, Carbohydr. Polym. 286 (2022) 119207, https://doi.org/10.1016/j.carbpol.2022.119207.
[48] S. Maity, N. Naskar, B. Jana, S. Lahiri, J. Ganguly, Fabrication of thiophene-chitosan hydrogel-trap for efficient immobilization of mercury (II) from aqueous environs, Carbohydr. Polym. 251 (2021) 116999, https://doi.org/10.1016/j.carbpol.2020.116999.
[49] A.U. Metin, E. Alver, Fibrous polymer-grafted chi-tosan/clay composite beads as a carrier for im-mobilization of papain and its usability for mercury elimination, Biopro-cess Biosyst. Eng. 39 (2016) 1137–1149, https://doi.org/10.1007/s00449-016-1590-0.
[50] A. Azari, H. Gharibi, B. Kakavandi, G. Ghanizadeh, A. Javid, A.H. Mahvi, K. Sharafi, T. Khosravia, Magnetic adsorption separation process: an alterna-tive method of mercury extracting from aqueous solution using modified chitosan coated Fe3O4 nanocomposites, J. Chem. Technol. Biotechnol. 92 (2017) 188–200, https://doi.org/10.1002/jctb.4990.
[51] E.V. Liakos, M. Mone, D.A. Lambropoulou, D.N. Bikiaris, G. Z. Kyzas, Adsorption evaluation for the removal of nickel, mercury, and barium ions from single-component and mixtures of aqueous solu-tions by using an optimized bio-based chitosan de-rivative, Polymers 13 (2021) 232, https://doi.org/10.3390/polym13020232.
[52] R.E. Kurdi, M. Chebl, M. Sillanpää, H. El-Rassy, D. Patra, Chitosan oligosaccharide/silica nanoparticles hybrid porous gel for mercury adsorption and detec-tion, Mater. Today Commun. 28 (2021) 102707, https://doi.org/10.1016/j.mtcomm.2021.102707.